

## A White Dwarf with Transiting Circumstellar Material Far Outside Its Tidal Disruption Radius

Z. VANDERBOSCH,<sup>1,2</sup> J. J. HERMES,<sup>3</sup> E. DENNIHY,<sup>4</sup> B. H. DUNLAP,<sup>1</sup> P. IZQUIERDO,<sup>5,6</sup> P.-E. TREMBLAY,<sup>7</sup> P. B. CHO,<sup>1,2</sup> B. T. GÄNSICKE,<sup>7</sup> K. J. BELL,<sup>8,9</sup> M. H. MONTGOMERY,<sup>1,2</sup> AND D. E. WINGET<sup>1,2</sup><sup>1</sup>Department of Astronomy, University of Texas at Austin, Austin, TX-78712, USA<sup>2</sup>McDonald Observatory, Fort Davis, TX-79734, USA<sup>3</sup>Department of Astronomy, Boston University, Boston, MA-02215, USA<sup>4</sup>Gemini Observatory, Casilla 603, La Serena, Chile<sup>5</sup>Instituto de Astrofísica de Canarias, 38205 La Laguna, Tenerife, Spain<sup>6</sup>Departamento de Astrofísica, Universidad de La Laguna, 38206 La Laguna, Tenerife, Spain<sup>7</sup>Department of Physics, University of Warwick, Coventry CV4 7AL, UK<sup>8</sup>DIRAC Institute, Department of Astronomy, University of Washington, Seattle, WA-98195, USA<sup>9</sup>NSF Astronomy and Astrophysics Postdoctoral Fellow

Submitted to ApJL

## ABSTRACT

We report the discovery of a white dwarf exhibiting deep, irregularly shaped transits indicative of disrupted planetary debris. Two prominent transits are seen in the 210-day-long Zwicky Transient Facility light curve of ZTF J013906.17+524536.89, each roughly 25 days long and causing 30–45% dips in flux. The transits are separated by about 110 days, much longer than the 4.5 hour orbital period observed in WD1145+017, the only other white dwarf with transiting circumstellar debris. An eccentricity  $e > 0.97$  is required assuming a 110-day orbital period and material that comes within the white dwarf’s tidal disruption radius, suggesting an early phase of tidal disruption prior to complete disk filling. An optical spectrum of ZTF J0139+5245 reveals strong Balmer lines, establishing it as a DA white dwarf with  $T_{\text{eff}} = 10,530 \pm 140$  K and  $\log(g) = 7.86 \pm 0.06$ . The spectroscopic  $T_{\text{eff}}$  combined with broadband photometry suggests a high extinction towards ZTF J0139+5245. A Ca II absorption feature at 3934 Å is present in all three nights of spectra, but its association with ZTF J0139+5245 remains uncertain. In addition, high-speed time series photometry is suggestive of short-period (950 s) variability, consistent with ZZ Ceti pulsations.

*Keywords:* white dwarf — eclipse — transits — debris disk — circumstellar dust — tidal disruption

## 1. INTRODUCTION

The vast majority of currently known planet hosts will one day become white dwarfs (WDs), the end products of stellar evolution for low- to intermediate-mass stars ( $M < 10 M_{\odot}$ ) (Williams et al. 2009). Many planets are expected to survive the post-main-sequence evolution of their host stars (Veras 2016). Indeed, at least one third of all known WDs with  $T_{\text{eff}} < 20,000$  K exhibit heavy elements beyond hydrogen and helium in their photospheres (Zuckerman et al. 2010; Koester et al. 2014), which is commonly interpreted as the active accretion of tidally disrupted planetary debris (Debes & Sigurds-

son 2002; Jura 2003; Zuckerman et al. 2010; Veras et al. 2014; Farihi 2016; Mustill et al. 2018).

This debris has been detected in more than 40 WDs as an infrared (IR) excess indicative of circumstellar dust, while gas disks are detected in a small number of these systems via Ca II triplet emission (Farihi 2016). Only two WDs, however, exhibit evidence for intact planetesimals in close orbit: WD1145+017 (Vanderburg et al. 2015), which displays photometric and spectroscopic signatures of transiting debris in 4.5–4.9 hour orbits; and SDSS J1228+1040 (Manser et al. 2019), which shows 2-hour variations in the Ca II triplet emission lines consistent with perturbations of a gas disk by a minor planet.

In this Letter, we report the discovery of a WD (ZTF J013906.17+524536.89, hereafter J0139) exhibit-

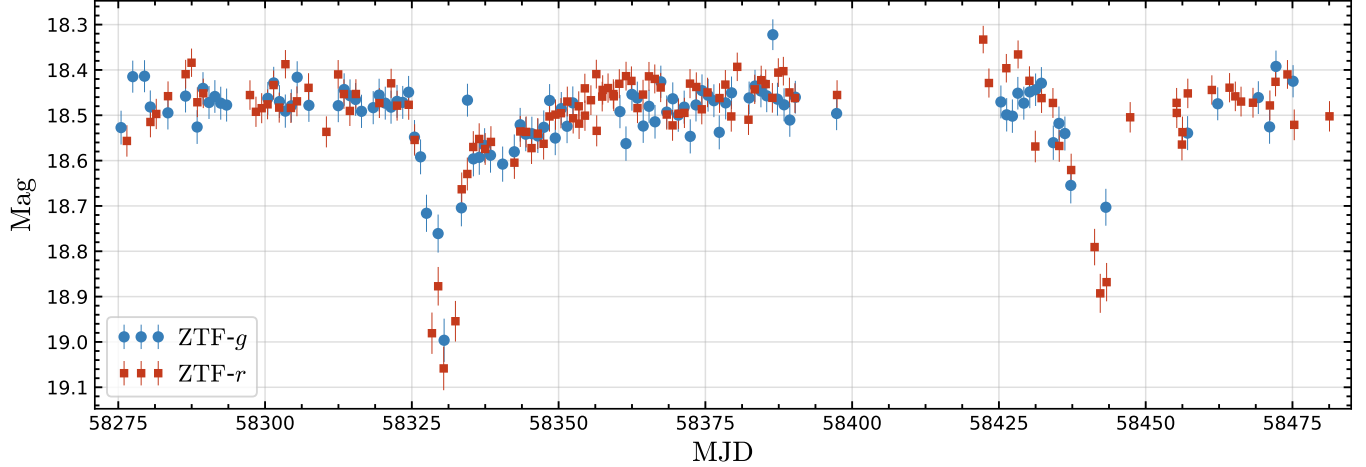


**Figure 1.** The light curve for J0139 from the first ZTF public data release. Magnitudes measured in the ZTF  $g$  and  $r$  bands are indicated with blue circles and red squares, respectively.

ing photometric evidence for transits caused by tidally disrupted, circumstellar debris. The two irregularly shaped 30–45% photometric dips observed by the Zwicky Transient Facility are separated by 110-days and each last roughly 25 days, consistent with circumstellar material in an early phase of tidal disruption along a highly eccentric orbit (Veras et al. 2014). In the following sections, we present publicly archived and newly obtained photometry and spectroscopy to constrain the white dwarf and its circumstellar material.

## 2. OBSERVATIONS

### 2.1. Public ZTF Photometry

We discovered transits in J0139 ( $g=18.5$ ) during a general search for variable WDs in the public Zwicky Transient Facility (ZTF) survey (Masci et al. 2019; Bellm et al. 2019) by cross-matching the *Gaia* DR2 catalogue of WDs (Gentile Fusillo et al. 2019, hereafter GF19) with the public ZTF transient alert database (Patterson et al. 2019) using the API provided by the Las Cumbres Observatory’s Make Alerts Really Simple (MARS) project<sup>1</sup>. Prior to the cross-match, we trimmed the full GF19 catalogue into an astrometrically clean, 200 pc sample of  $\approx 40,000$  objects using the criteria recommended by Lindegren et al. (2018) and Evans et al. (2018). As of 2019 May 08, this cross match results in 783 objects which have at least one alert from ZTF indicative of transient or periodically variable behavior. We downloaded the public ZTF light curves for each object with an alert and visually inspected them and their periodograms for signs of variability. J0139 stood out

as the only object with long-lasting, well-defined dips in flux (see Fig. 1).

In total, J0139 was covered by 234 public ZTF observations deemed of good photometric quality by the ZTF pipeline. We filtered these observations by only selecting points where *catflags* = 0, a condition for generating clean light curves recommended in the ZTF Science Data System Explanatory Supplement<sup>2</sup>. The final light curve for J0139, shown in Figure 1, has 224 data points (104 in  $g$  and 120 in  $r$ ) with a median temporal separation between observations of 22.4 hours with occasional large, multi-day gaps.

### 2.2. Spectroscopy

We obtained the first spectra of J0139 (see Fig. 2) on 2019 June 30, July 3, and July 4 using the Intermediate-dispersion Spectrograph and Imaging System (ISIS), mounted on the 4.2-m William Herschel Telescope (WHT) on the island of La Palma, Spain.

We performed the observations using a  $1''$  slit and 600 line  $\text{mm}^{-1}$  grating in the blue ( $3800$ – $5200$  Å) arm of the spectrograph, achieving  $1.9$  Å resolution. Each night we took a series of consecutive 1200s exposures under clear sky conditions with seeing between  $0.6''$  –  $1.0''$  and an average airmass of 1.5. We obtained a total of 17 20-minute exposures for a combined exposure time of 5.7 hours.

We applied bias, flat-field, and cosmic ray corrections to our spectra using standard procedures within IRAF. We optimally extracted the one-dimensional spectrum (Horne 1986) using the data reduction software PAMELA.

<sup>1</sup> <https://mars.lco.global/>

<sup>2</sup> [http://web.ipac.caltech.edu/staff/fmasci/ztf/ztf\\_pipelines-deliverables.pdf](http://web.ipac.caltech.edu/staff/fmasci/ztf/ztf_pipelines-deliverables.pdf)

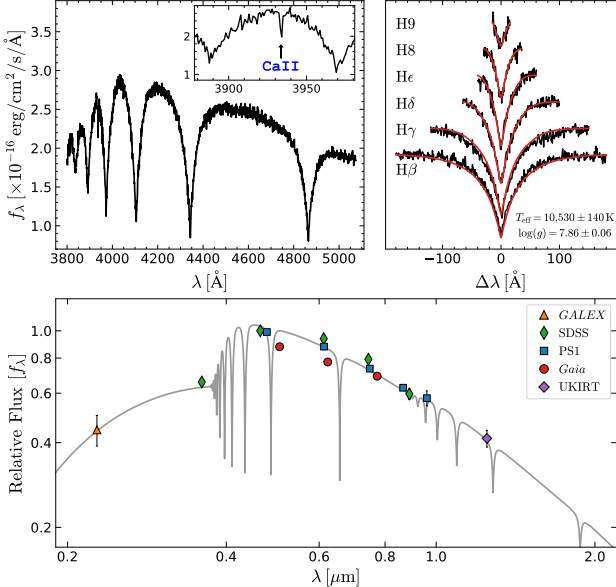


**Figure 2.** The WHT/ISIS optical spectrum and SED of J0139. The top left panel shows the combined spectrum for all three nights of observations with an inset plot highlighting the Ca II absorption feature at 3934Å. The top right panel shows the fit to the six Balmer lines, H $\beta$  – H9, from which we derive spectroscopic  $\log(g)$  and  $T_{\text{eff}}$  values (see Section 3.1). The bottom panel shows the SED with photometric data de-reddened using the reddening law of Fitzpatrick (1999) and Indebetouw et al. (2005) with  $E(B – V) = 0.12$  and  $A_V = 0.38$ . We over-plot a model spectrum (grey line, Koester 2010) with  $T_{\text{eff}} = 10,500$  K and  $\log(g) = 7.75$  representing a good match to the shape of the observed SED.

We used MOLLY (Marsh 1989) to wavelength and flux-calibrate the spectra by fitting a fourth-order polynomial to the HgArNeXe arc data and a five-knot spline to the spectrophotometric standard star, respectively. Arcs and standards were obtained using the same instrument setup just before and after the science observations were carried out.

### 2.3. McDonald & LCOGT Photometry

We began monitoring J0139 for additional transits on 2019 June 21 using the the Las Cumbres Observatory (LCOGT) 1.0-m telescope network and the McDonald Observatory 2.1-m Otto Struve Telescope (see Fig. 3).

For the LCOGT 1.0-m observations, we requested three 2-minute-long exposures in both  $gp$  and  $rp$  filters each night using the Sinistro imaging instrument (Brown et al. 2013). Completed observations were bias, dark, and flat-field corrected via the LCOGT BANZAI pipeline<sup>3</sup>. We wrote a custom Python script that per-

forms circular aperture photometry on all sources detected within each image and then cross-matches them with known Pan-STARRS1 Survey (PS1) sources. We measured the difference between PS1 and instrumental magnitudes ( $m_d = m_{\text{PS1}} - m_{\text{LCOGT}}$ ) while filtering for outliers and likely galaxy candidates. We converted our instrumental magnitudes to apparent magnitudes on the PS1 scale by solving for a zero-point offset ( $z$ ) and color term ( $c$ ) with a least squares fit to  $m_d = z + c(g_{\text{PS1}} - r_{\text{PS1}})$ .

From the McDonald 2.1-m telescope we acquired five nights of high-speed time-series photometry using the Princeton Instruments ProEM frame-transfer CCD with 30-s exposures. For the first two nights, we used only an Astrodon Gen2 Sloan  $g'$  filter. For the next three nights we alternated between  $g'$  and  $r'$  for each exposure using an automated filter wheel. We used IRAF to bias, dark, and flat-field correct the McDonald data using standard calibration frames taken before each night of observations. We performed circular aperture photometry to generate light curves using the IRAF routine CCD\_HSP (Kanaan et al. 2002). Lastly, we used the Wqed software suite to apply a barycentric correction to the mid-exposure timestamp of each image (Thompson & Mullally 2013).

### 2.4. SED & Single-Epoch Photometry

We compiled all available photometric and astrometric data for J0139 from the Galaxy Evolution Explorer (GALEX, Martin et al. 2005; Morrissey et al. 2005), Gaia DR2 (Gaia Collaboration et al. 2018), the Sloan Digital Sky Survey (SDSS) DR9 (Ahn et al. 2012), the Pan-STARRS1 Survey (Chambers et al. 2016) DR2, the United Kingdom Infra-Red Telescope (UKIRT) Hemisphere Survey (UHS, Dye et al. 2018), and the Wide-Field Infrared Survey Explorer (WISE, Wright et al. 2010). The compiled data are summarized in Table 1 while the spectral energy distribution (SED) is displayed in Fig. 2.

The PS1  $3\pi$  survey (Kaiser et al. 2010; Magnier et al. 2013) is multi-epoch, so we also obtained all single-epoch detections to look for additional transit events. In total, J0139 was observed by PS1 63 times over the course of 4.4 years. To filter out poor-quality detections, we first removed those where  $> 5\%$  of the fitted PSF model was contaminated by bad pixels. To further filter our data, we followed the methods of Fulton et al. (2014). The resulting PS1 light curve, shown in Figure 4, has 52 data points ( $g:11, r:9, i:11, z:10, y:11$ ) with 30 – 80 s exposure times.

WISE photometry was not reported for J0139 in the original AllWISE catalogue (Wright et al. 2010; Mainzer

<sup>3</sup> <https://github.com/LCOGT/banzai>

**Table 1.** ZTF J0139+5245 Summary of Properties

$\alpha, \delta$ (J2000)	01h39m06.17s +52d45m36.89s <sup>[1]</sup>	
$\mu_\alpha, \mu_\delta$ (mas/yr)	$87.32 \pm 0.39, 4.99 \pm 0.43$ <sup>[1]</sup>	
$\varpi$ (mas)	$5.77 \pm 0.25$ <sup>[1]</sup>	
$d$ (pc)	$172.9 \pm 7.4$ <sup>[1]</sup>	
$T_{\text{eff}}^{3D}$ (K)	$10,530 \pm 140$ <sup>[2]</sup>	
$\log(g)^{3D}$ (cgs)	$7.86 \pm 0.06$ <sup>[2]</sup>	
NUV	$19.89 \pm 0.14$ <sup>[3,4]</sup>	
$G$	$18.594 \pm 0.008$ <sup>[1]</sup>	
$G_{\text{BP}}$	$18.55 \pm 0.02$ <sup>[1]</sup>	
$G_{\text{RP}}$	$18.64 \pm 0.03$ <sup>[1]</sup>	
SDSS <sup>[5]</sup>	PS1 <sup>[6]</sup>	
$u$	$19.04 \pm 0.04$	
$g$	$18.46 \pm 0.01$	$18.48 \pm 0.01$
$r$	$18.40 \pm 0.01$	$18.49 \pm 0.01$
$i$	$18.52 \pm 0.01$	$18.59 \pm 0.01$
$z$	$18.75 \pm 0.04$	$18.69 \pm 0.02$
$y$		$18.78 \pm 0.03$
$J$	$19.10 \pm 0.07$ <sup>[7]</sup>	

[1] GF19, [2] This Work, [3] Martin et al. (2005),

[4] Morrissey et al. (2005), [5] Ahn et al. (2012),

[6] Chambers et al. (2016), [7] Dye et al. (2018),

NOTE – All magnitudes are on the AB scale. *Gaia* and UKIRT were converted from Vega to AB scales using the *Gaia* DR2 documentation<sup>a</sup> and Hewett et al. (2006).

<sup>a</sup><https://gea.esac.esa.int/archive/documentation/GDR2/>

et al. 2011). The “unWISE” catalogue (Lang et al. 2016), which contains forced photometry carried out on stacked *WISE* images at the locations of all SDSS optical sources, does report a detection for J0139 with Vega magnitudes of  $W1 = 17.20 \pm 0.09$  and  $W2 = 16.16 \pm 0.12$ . These detections are suggestive of an infrared (IR) excess for J0139, but due to the lack of an AllWISE detection, the absence of proper motion corrections in the Lang et al. (2016) forced photometry method, and the potential for contamination by line-of-sight objects, we consider this an unreliable IR excess detection and exclude it from the SED. Nonetheless, we discuss some of the implications for an IR excess throughout this Letter.

### 3. THE WHITE DWARF

#### 3.1. Physical Parameters

Prior to obtaining a spectrum, J0139 was considered a high probability WD candidate due to both its SDSS photometric colors (Girven et al. 2011) and its location in the *Gaia* color magnitude diagram (GF19). Utilizing *Gaia* photometry and parallax, GF19 report  $T_{\text{eff}} = 9420 \pm 580$  K,  $\log(g) = 7.87 \pm 0.21$ , and  $M = 0.52 \pm 0.11 M_\odot$  for J0139 assuming a pure-H atmosphere.

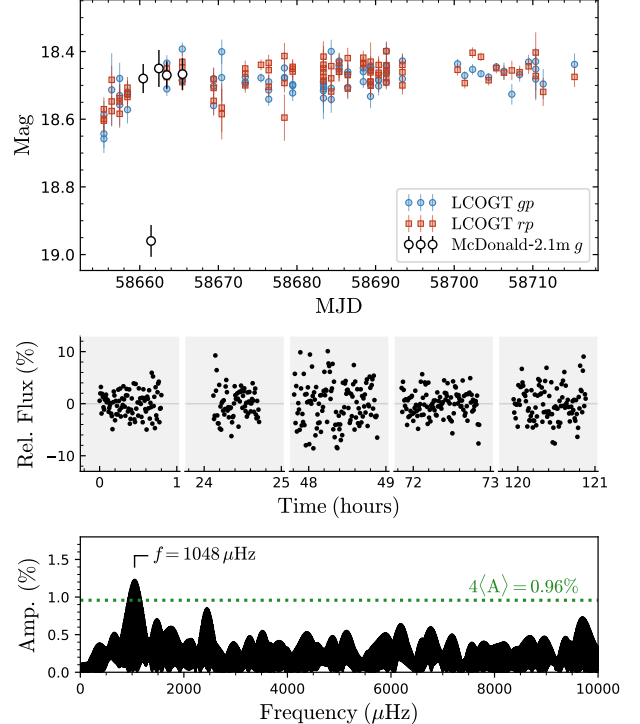


**Figure 3.** The McDonald 2.1-m and LCOGT 1.0-m photometry. The top panel shows the McDonald  $g$ -data (open circles) averaged for each night and scaled to the two nights of simultaneous LCOGT  $gp$ -data (blue circles) along with the LCOGT  $rp$ -data (red squares). The middle panel shows only the McDonald high-speed  $g$  and  $r$  photometry, normalized relative to six comparison stars within the field of view. The bottom panel shows the Lomb Scargle Periodogram of the high-speed McDonald photometry. The  $4\langle A \rangle$  significance threshold is shown by the green dotted line.

The newly obtained spectra provide clear evidence that J0139 is indeed a WD with a hydrogen-dominated atmosphere, hence a DA (see Fig. 2). We also detect a weak Ca II absorption feature at  $3934\text{\AA}$  in each night’s spectrum, but its origin (photospheric, circumstellar, or interstellar) remains unclear due to the large uncertainties in its velocity relative to the Balmer lines imposed by our relatively low spectral resolution.

Using the combined spectrum for all three nights of WHT observations, we fit six Balmer lines,  $H\beta - H9$ , utilizing the one-dimensional (1D) models and fitting procedures described in Tremblay et al. (2011) (see Fig. 2). We find  $T_{\text{eff}}^{1D} = 10790 \pm 140$  K and  $\log(g)^{1D} = 8.09 \pm 0.06$  whose formal uncertainties have been added in quadrature to 1.2%  $T_{\text{eff}}$  and 0.038-dex  $\log(g)$  uncertainties to account for typical systematics (Liebert et al. 2005). We apply corrections to these 1D values based on the three-dimensional (3D) convection simulations of Tremblay et al. (2013) to obtain  $T_{\text{eff}}^{3D} = 10530 \pm 140$  K and

$\log(g)^{3D} = 7.86 \pm 0.06$ . Utilizing the 3D values and the WD evolutionary models of [Fontaine et al. \(2001\)](#) with evenly mixed C/O cores and thick-H layers, we obtain  $M = 0.52 \pm 0.03 M_{\odot}$ .

The spectroscopic temperature is significantly hotter than the *Gaia* photometry and parallax determination of [GF19](#). [GF19](#) use a distance-scaling relationship to estimate extinction which performs well in general but may do poorly along lines of sight (LOS) where the Galactic extinction is high, which is true for J0139:  $A_{V,LOS} = 0.84$  ([Schlafly & Finkbeiner 2011](#)). [GF19](#) use  $A_V = 0.11$  in the photometric fit of J0139, but with  $A_V = 0.38$  we find good agreement between the observed and model SEDs at the best-fit spectroscopic temperature (see Fig. 2). This additional extinction could be accounted for by locally dense regions within the ISM, but J0139 is relatively nearby ( $d = 172.9 \pm 7.4$  pc, [Bailer-Jones et al. 2018](#)). Circumstellar material around J0139 could also account for the additional extinction, a possibility supported by the irregularly shaped transits and the potential for an IR excess and atmospheric/circumstellar Ca II absorption (see Sec. 4.3).

### 3.2. Short-Period Variability

The 3D spectroscopic  $T_{\text{eff}}$  and  $\log(g)$  place J0139 inside the ZZ Ceti instability strip ([Gianninas et al. 2015](#)) where hydrogen-atmosphere WDs pulsate. In the combined five-night McDonald light curve, we find a peak in the Lomb-Scargle periodogram at  $1048 \mu\text{Hz}$  (954 s) with an amplitude of 1.2% (see Fig. 3). We calculate a significance threshold of 0.96% using four times the average amplitude of the periodogram,  $4\langle A \rangle$ , between 500 and  $10,000 \mu\text{Hz}$ . The peak is therefore significant and has a period consistent with red-edge ZZ Cetis ([Mukadam et al. 2006](#)). However, due to the short individual runs and because we find only one significant peak, we note that other effects such as short-timescale transit variability, artifacts from atmospheric transparency variations, or stellar rotation could produce the observed peak, though WD's with spin periods  $< 1000$  s are very rare ([Hermes et al. 2017](#)).

## 4. THE CIRCUMSTELLAR MATERIAL

### 4.1. The Transit Spacing

With 210 days of photometry in the first public ZTF data release, only two sparsely sampled transits are observed (Fig. 1). We constrain the transit spacing by phase-folding the ZTF data to obtain a close match between the transit profiles of both events. This occurs with a folding period of  $\approx 110$  days. We searched for additional transits among the 52 good-quality PS1 data points, but find no indication of a transit detection dis-

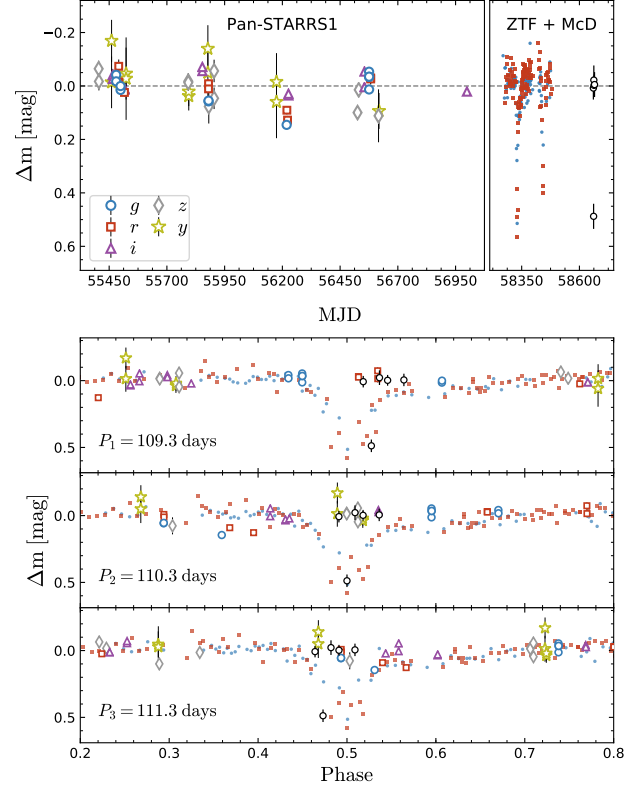


**Figure 4.** PS1 (Pan-STARRS1), ZTF, and McDonald photometry. The top row shows the photometry at each epoch represented by the change in magnitude with respect to the mean PS1 magnitude in each filter ( $g = 18.48$ ,  $r = 18.49$ ,  $i = 18.59$ ,  $z = 18.69$ ,  $y = 18.78$ ). PS1 is represented by colored open symbols, ZTF by small filled symbols, and McDonald by black open circles. The bottom rows show three period-folded light curves, each using a different period (see Section 4.1 for details on choice of periods) and shifted in phase so that the lowest ZTF data point has a phase of 0.5. Only phases between 0.2 and 0.8 are shown so the transit portion can be seen more clearly.

tinguishable from statistical noise ( $\Delta m > 0.15$  mag). As of 2019 August 19, we also see no evidence for deep transits from LCOGT, although the flux does appear to steadily increase during the first four nights of LCOGT observations (see Fig. 3).

During the 1-hour of McDonald 2.1-m observations on 2019 June 27, however, we observed a drop in flux of  $\approx 0.45$  mag relative to neighboring nights (see Fig. 3). This drop occurs 331 days, or three 110.3-day cycles, after the deepest part of the first ZTF transit. We use this 110.3-day period, along with  $\pm 1$  day options, to fold the PS1, ZTF, and McDonald light curves together (see Fig. 4).

Interestingly, while all three folding periods provide decent agreement between ZTF transits and the single low-lying McDonald point, the remaining McDonald and

PS1 data exhibit obvious discrepancies. This may indicate the absence of periodic behavior, but is also reminiscent of WD1145+017 which exhibits periodic transits with both orbit-to-orbit ( $4.5 < P_{\text{orb}} < 4.9$  hours) and years-long dynamical evolution of their shapes and depths (Vanderburg et al. 2015; Gänsicke et al. 2016; Rappaport et al. 2018). KIC 8463852, an F-type main sequence star with dust-induced transits, also shows irregularly shaped transits that have yet to exhibit conclusively periodic behavior over several years of observations (Boyajian et al. 2016; Schaefer et al. 2018).

#### 4.2. A Potential Orbital Configuration

To account for the presence of transits in J0139, we consider the model where a small rocky object, such as an asteroid, was at some point perturbed off its original orbit and brought close enough to the WD to be tidally disrupted into a stream of dust and debris (Debes & Sigurdsson 2002; Veras et al. 2013). Assuming the observed ZTF transit spacing is the orbital period of that debris, and that the material is currently orbiting near to or within the tidal disruption radius ( $r_c$ ) at closest approach, a very high eccentricity is required.

Using standard estimates for the average densities of asteroids and planets ( $\rho = 2.0 - 8.0 \text{ g/cm}^3$ ) and the ratios between their central and average densities ( $\rho_c/\rho = 1.0 - 2.5$ ), we find  $r_c$  for J0139 to be between 1.0 and 1.7 solar radii (Rappaport et al. 2013). Using  $r_c$  as the distance of closest approach implies an eccentricity of  $e > 0.97$  and a maximum orbital separation of  $\approx 0.72 \text{ AU}$ .

At periastron, a single dust grain would take  $< 1$ -minute to transit the WD, and at apastron 1 – 2 hours. Much longer transits are observed by ZTF, suggesting the presence of an extended disrupted stream of dust and/or debris. Large planetesimals may be embedded within this material, but our current constraints on rapid transits from ZTF and McDonald are weak due to sparse coverage.

We can estimate a lower limit on the mass of the transiting material which passes between the WD and Earth by assuming the transit is caused by non-overlapping spherical particles. The total amount of WD light blocked during the first ZTF transit is equivalent to a total eclipse lasting four days. If transiting at a distance of  $1.0 R_{\odot}$ , the required dust mass is  $M_d = 10^{19} \left( \frac{r_d}{1 \mu\text{m}} \right) \left( \frac{\rho_d}{2 \text{ g/cm}^3} \right) \text{g}$ , where  $r_d$  and  $\rho_d$  are the radius and density of a single dust grain. If transiting at  $0.72 \text{ AU}$  the estimate decreases to  $M_d = 10^{17} \left( \frac{r_d}{1 \mu\text{m}} \right) \left( \frac{\rho_d}{2 \text{ g/cm}^3} \right) \text{g}$ . In both cases the masses are consistent with asteroid-sized objects.

#### 4.3. Evidence for Dust and Accretion

In addition to the irregularly shaped transits, we also find evidence from the “unWISE” photometry for an IR excess. Though we are skeptical of its association with J0139, a single-temperature blackbody fit to the excess (Dennihy et al. 2017) gives  $T_{\text{BB}} = 650 \text{ K}$  and  $R_{\text{BB}} = 35 R_{\text{WD}}$ . A brown dwarf companion ( $R \approx 0.1 R_{\odot}$ ) at the same temperature would be a factor of  $\approx 20$  less luminous (Sorahana et al. 2013). Warm dust provides a more likely explanation, but source confusion/contamination cannot be ruled out.

To date, all WDs with a confirmed infrared excess also show signs of atmospheric metal pollution from accretion of this debris (Farihi 2016). We identified an absorption feature near the  $3934 \text{ \AA}$  Ca II transition on all three nights of spectroscopic observations (see Fig. 2), but as mentioned in Section 3, our knowledge of its origin (photospheric, circumstellar, or interstellar) remains poorly constrained.

#### 4.4. Implications for Tidal Disruption

If the observed transits in J0139 are indeed caused by orbiting disrupted planetary debris, it would be just the second such object known. In comparison to WD1145+017, however, J0139 presents unique challenges related to its potential orbital configuration.

Completely tidally disrupted asteroids on highly eccentric orbits are expected to uniformly fill a dust disk on timescales much shorter than WD cooling times (Debes et al. 2012; Veras et al. 2014). The disruption and disk-filling timescales depend non-trivially, however, on factors such as the original size, composition, and spin rate of the pre-disruption object, how close it gets to the tidal disruption boundary, and the effect of inter-particle collisions throughout the disruption process (Debes et al. 2012; Veras et al. 2014, 2017; Kenyon & Bromley 2017; Makarov & Veras 2019). All of these factors remain poorly constrained or completely unknown for J0139, but the observed transits suggest J0139 is still early in the disruption process, prior to complete disk filling, making it an interesting case study for the physics and evolutionary timescales involved in the tidal disruption of planetary objects around WDs.

In addition, we note that J0139’s mass ( $M = 0.52 M_{\odot}$ ) is consistent with forming from a relatively low mass progenitor star ( $\approx 1.2 M_{\odot}$ , El-Badry et al. 2018). This implies a progenitor age ( $\approx 12 \text{ Gyr}$ , Kalirai 2012) and WD cooling age (500 Myr, Fontaine et al. 2001) that are both older relative to most WDs with detectable IR excesses (Rocchetto et al. 2015). The survivability of extrasolar asteroid belts around low-mass stars which contain enough material to account for ongoing tidal

disruption events, IR excesses, and metal accretion is still an open question (Farihi 2016).

## 5. CONCLUSIONS

We have presented the discovery of a WD exhibiting photometric evidence for transits caused by tidally disrupted planetary debris. We have placed loose constraints on the transit recurrence time ( $\approx 110$  days) and potential eccentricity ( $e > 0.97$ ) of the transiting material assuming that it orbits near to or within the tidal disruption radius of the WD. We obtained the first spectrum of J0139 which identifies the WD as a DA due to strong Balmer lines. We detect an absorption feature near the 3934Å Ca II line in all three nights of spectra and find evidence for an IR excess consistent with warm dust, but their association with the WD remains uncertain. *Spitzer* observations are needed to reliably constrain J0139's infrared flux, while high-resolution spectroscopy is needed to properly constrain the relative radial velocities of the Ca II and Balmer lines.

Future data releases from ZTF will hopefully reveal more transits in the light curve of J0139. In the meantime, we have begun a photometric observing program using the McDonald 2.1m telescope and the LCOGT network to obtain both high-speed time-series photometry and nightly monitoring of J0139. More extensive observations, such as multi-color time series photometry and infrared and optical spectroscopy in and out of transit, are required to better understand the nature of the WD and its transiting material. In addition, WD1145+017 is also among the 783 objects in our *Gaia*-ZTF cross match. We expect a more systematic search of a larger space volume of WDs in ZTF, and in future surveys such as the Large Synoptic Survey Telescope (LSST), will yield many more discoveries like J0139 and WD1145+017.

## 6. ACKNOWLEDGEMENTS

The authors would like to thank J. Farihi for providing useful feedback on a draft of this Letter, D. Koester for the use of his models, and T. Marsh for developing and making available both PAMELA and MOLLY. Data from McDonald Observatory were obtained with financial support from NASA K2 Cycle 5 Grant 80NSSC18K0387 and the Wooten Center for Astrophysical Plasma Properties (WCAPP) under DOE grant DE-FOA-0001634. BTG was supported by the UK STFC grant ST/P000495. This material is based upon work supported by the National Science Foundation under Award AST-1903828. The research leading to these results has received funding from the European Research Council under the European Unions Horizon 2020 research and innovation programme n. 677706 (WD3D).

This work is based on observations obtained with the Samuel Oschin 48-inch Telescope at the Palomar Observatory as part of the Zwicky Transient Facility project which is supported by NSF Grant No. AST-1440341 and the participating institutions of the ZTF collaboration. We make use of observations and reduction software from the Las Cumbres Observatory (LCOGT) network, and include data from the Pan-STARRS1 Surveys (PS1) and the PS1 public science archive which have been made possible through contributions by participating institutions of the PS1 collaboration (<https://panstarrs.stsci.edu/>).

We also make use of data from the Wide-field Infrared Survey (WISE, <http://wise2.ipac.caltech.edu/docs/release/allsky>), the United Kingdom Infra-Red Telescope from the year 2016 (UKIRT, <http://www.ukirt.hawaii.edu/>), the NASA Galaxy Evolution Explorer (GALEX, <http://www.galex.caltech.edu/>), the SDSS-III (<http://www.sdss3.org/>), and from the European Space Agency (ESA) mission *Gaia* (<https://www.cosmos.esa.int/gaia>) processed by the *Gaia* Data Processing and Analysis Consortium (DPAC, <https://www.cosmos.esa.int/web/gaia/dpac/consortium>).

## REFERENCES

Ahn, C. P., Alexandroff, R., Allende Prieto, C., et al. 2012, *ApJS*, 203, 21

Bailer-Jones, C. A. L., Rybizki, J., Fouesneau, M., Mantelet, G., & Andrae, R. 2018, *AJ*, 156, 58

Bellm, E. C., Kulkarni, S. R., Graham, M. J., et al. 2019, *PASP*, 131, 018002

Boyajian, T. S., LaCourse, D. M., Rappaport, S. A., et al. 2016, *MNRAS*, 457, 3988

Brown, T. M., Baliber, N., Bianco, F. B., et al. 2013, *PASP*, 125, 1031

Chambers, K. C., Magnier, E. A., Metcalfe, N., et al. 2016, arXiv e-prints, arXiv:1612.05560

Debes, J. H., & Sigurdsson, S. 2002, *ApJ*, 572, 556

Debes, J. H., Walsh, K. J., & Stark, C. 2012, *ApJ*, 747, 148

Dennihy, E., Clemens, J. C., Debes, J. H., et al. 2017, *ApJ*, 849, 77

Dye, S., Lawrence, A., Read, M. A., et al. 2018, MNRAS, 473, 5113

El-Badry, K., Rix, H.-W., & Weisz, D. R. 2018, The Astrophysical Journal, 860, L17

Evans, D. W., Riello, M., De Angeli, F., et al. 2018, A&A, 616, A4

Farihi, J. 2016, NewAR, 71, 9

Fitzpatrick, E. L. 1999, PASP, 111, 63

Fontaine, G., Brassard, P., & Bergeron, P. 2001, PASP, 113, 409

Fulton, B. J., Tonry, J. L., Flewelling, H., et al. 2014, ApJ, 796, 114

Gaia Collaboration, Brown, A. G. A., Vallenari, A., et al. 2018, A&A, 616, A1

Gänsicke, B. T., Aungwerojwit, A., Marsh, T. R., et al. 2016, ApJL, 818, L7

Gentile Fusillo, N. P., Tremblay, P.-E., Gänsicke, B. T., et al. 2019, MNRAS, 482, 4570

Gianninas, A., Kilic, M., Brown, W. R., Canton, P., & Kenyon, S. J. 2015, ApJ, 812, 167

Girven, J., Gänsicke, B. T., Steeghs, D., & Koester, D. 2011, MNRAS, 417, 1210

Hermes, J. J., Gänsicke, B. T., Kawaler, S. D., et al. 2017, The Astrophysical Journal Supplement Series, 232, 23

Hewett, P. C., Warren, S. J., Leggett, S. K., & Hodgkin, S. T. 2006, MNRAS, 367, 454

Horne, K. 1986, PASP, 98, 609

Indebetouw, R., Mathis, J. S., Babler, B. L., et al. 2005, ApJ, 619, 931

Jura, M. 2003, ApJ, 584, L91

Kaiser, N., Burgett, W., Chambers, K., et al. 2010, in Society of Photo-Optical Instrumentation Engineers (SPIE) Conference Series, Vol. 7733, Proc. SPIE, 77330E

Kalirai, J. S. 2012, Nature, 486, 90

Kanaan, A., Kepler, S. O., & Winget, D. E. 2002, A&A, 389, 896

Kenyon, S. J., & Bromley, B. C. 2017, ApJ, 844, 116

Koester, D. 2010, Mem. Soc. Astron. Italiana, 81, 921

Koester, D., Gänsicke, B. T., & Farihi, J. 2014, A&A, 566, A34

Lang, D., Hogg, D. W., & Schlegel, D. J. 2016, AJ, 151, 36

Liebert, J., Bergeron, P., & Holberg, J. B. 2005, ApJS, 156, 47

Lindegren, L., Hernández, J., Bombrun, A., et al. 2018, A&A, 616, A2

Magnier, E. A., Schlafly, E., Finkbeiner, D., et al. 2013, ApJS, 205, 20

Mainzer, A., Bauer, J., Grav, T., et al. 2011, ApJ, 731, 53

Makarov, V. V., & Veras, D. 2019, arXiv e-prints, arXiv:1908.04612

Manser, C. J., Gänsicke, B. T., Eggl, S., et al. 2019, Science, 364, 66

Marsh, T. R. 1989, PASP, 101, 1032

Martin, D. C., Fanson, J., Schiminovich, D., et al. 2005, ApJL, 619, L1

Masci, F. J., Laher, R. R., Rusholme, B., et al. 2019, PASP, 131, 018003

Morrissey, P., Schiminovich, D., Barlow, T. A., et al. 2005, ApJL, 619, L7

Mukadam, A. S., Montgomery, M. H., Winget, D. E., Kepler, S. O., & Clemens, J. C. 2006, ApJ, 640, 956

Mustill, A. J., Villaver, E., Veras, D., Gänsicke, B. T., & Bonsor, A. 2018, MNRAS, 476, 3939

Patterson, M. T., Bellm, E. C., Rusholme, B., et al. 2019, PASP, 131, 018001

Rappaport, S., Gary, B. L., Vanderburg, A., et al. 2018, MNRAS, 474, 933

Rappaport, S., Sanchis-Ojeda, R., Rogers, L. A., Levine, A., & Winn, J. N. 2013, ApJL, 773, L15

Rocchetto, M., Farihi, J., Gänsicke, B. T., & Bergfors, C. 2015, Monthly Notices of the Royal Astronomical Society, 449, 574. <https://doi.org/10.1093/mnras/stv282>

Schaefer, B. E., Bentley, R. O., Boyajian, T. S., et al. 2018, MNRAS, 481, 2235

Schlafly, E. F., & Finkbeiner, D. P. 2011, ApJ, 737, 103

Sorahana, S., Yamamura, I., & Murakami, H. 2013, ApJ, 767, 77

Thompson, S., & Mullally, F. 2013, Astrophysics Source Code Library, ascl:1304.004

Tremblay, P. E., Bergeron, P., & Gianninas, A. 2011, ApJ, 730, 128

Tremblay, P. E., Ludwig, H. G., Steffen, M., & Freytag, B. 2013, A&A, 559, A104

Vanderburg, A., Johnson, J. A., Rappaport, S., et al. 2015, Nature, 526, 546

Veras, D. 2016, Royal Society Open Science, 3, 150571

Veras, D., Carter, P. J., Leinhardt, Z. M., & Gänsicke, B. T. 2017, MNRAS, 465, 1008

Veras, D., Leinhardt, Z. M., Bonsor, A., & Gänsicke, B. T. 2014, MNRAS, 445, 2244

Veras, D., Mustill, A. J., Bonsor, A., & Wyatt, M. C. 2013, MNRAS, 431, 1686

Williams, K. A., Bolte, M., & Koester, D. 2009, ApJ, 693, 355

Wright, E. L., Eisenhardt, P. R. M., Mainzer, A. K., et al. 2010, AJ, 140, 1868

Zuckerman, B., Melis, C., Klein, B., Koester, D., & Jura, M. 2010, ApJ, 722, 725